Journal of Nuclear Materials 389 (2009) 410–415

Contents lists available at ScienceDirect

Journal of Nuclear Materials

journal homepage: www.elsevier.com/locate/jnucmat

In situ studies of ion irradiated inverse spinel compound magnesium stannate (Mg_2SnO_4)

P. Xu [a,*], M. Tang [b], J.C. Nino [a]

[a] Department of Materials Science and Engineering, University of Florida, 100 Rhines Hall, Gainesville, Florida 32611, USA
[b] Materials Science and Technology Division, Los Alamos National Laboratory, Los Alamos, New Mexico 87545, USA

ARTICLE INFO

Article history:
Received 18 September 2008
Accepted 8 February 2009

ABSTRACT

Magnesium stannate spinel (Mg_2SnO_4) was synthesized through conventional solid state processing and then irradiated with 1.0 MeV Kr^{2+} ions at low temperatures 50 and 150 K. Structural evolutions during irradiation were monitored and recorded through bright field images and selected-area electron diffraction patterns using *in situ* transmission electron microscopy. The amorphization of Mg_2SnO_4 was achieved at an ion dose of 5×10^{19} Kr ions/m^2 at 50 K and 10^{20} Kr ions/m^2 at 150 K, which is equivalent to an atomic displacement damage of 5.5 and 11.0 dpa, respectively. The spinel crystal structure was thermally recovered at room temperature from the amorphous phase caused by irradiation at 50 K. The calculated electronic and nuclear stopping powers suggest that the radiation damage caused by 1 MeV Kr^{2+} ions in Mg_2SnO_4 is mainly due to atomic displacement induced defect accumulation. The radiation tolerance of Mg_2SnO_4 was finally compared with normal spinel $MgAl_2O_4$.

Published by Elsevier B.V.

1. Introduction

There is an increasing inventory of radioactive nuclear waste from both spent nuclear fuels and weapon programs, such as plutonium and minor actinides. Inert matrix (IM) materials are proposed to dispose the radioactive materials and to generate electricity in a safe and ecological manner [1,2]. The prototype spinel compound, magnesium aluminate ($MgAl_2O_4$), has attracted much attention as a potential IM material due to its good stability against ballistic displacements caused by neutron or low energy ion irradiation [3–7]. It has been reported that the amorphization dose of $MgAl_2O_4$ under irradiation of 1.5 MeV Xe^+ ions at 30 K is equivalent to 35–40 displacement per atom (dpa) [8]. The mechanisms underlying the radiation resistance of the spinel structure have been determined as cation disorder (anti-site defects) [9] and interstitial–vacancy (i–v) recombination [10]. Moreover, $MgAl_2O_4$ is a complex oxide compound with two types of cations in the structure. It has been suggested that this multi-component chemistry suppresses the nucleation and growth of interstitial dislocation loops during irradiation [4]. However, $MgAl_2O_4$ swells in in-pile irradiation tests, which excludes it from utilization as an IM material. Recent studies suggest that the swelling may be attributed to fission fragment induced damage and amorphization [11–13], but the mechanisms are not well understood. Other spinel compounds may exhibit good irradiation resistance to both ballistic displacement and fission fragment damage, thus the radiation behavior of compounds with spinel crystal structure is worth further investigation.

Wang and his co-workers [14] have compared the irradiation stability of several X_2YO_4 compounds with olivine and spinel structure. It has been found that the compounds with spinel structure in general are more irradiation "resistant" than the olivine compounds; and among the irradiated spinels, $MgAl_2O_4$ is more "resistant" than $FeCr_2O_4$ and γ-$SiFe_2O_4$. The irradiation behavior of some other spinel compounds, such as $MgCr_2O_4$, $ZnAl_2O_4$, $ZnFe_2O_4$, $MgFe_2O_4$, $NiFe_2O_4$, Fe_3O_4, $MgGa_2O_4$, and $MgIn_2O_4$, has also been studied either experimentally or theoretically using computer simulation [15–21]. In search for potential irradiation "resistant" spinel compounds, magnesium stannate (Mg_2SnO_4) was selected in this work and its irradiation stability was assessed for a screening type of study.

The existence of the stable phase Mg_2SnO_4 has been described by several authors, and dense polycrystalline Mg_2SnO_4 can be achieved by sintering at 1873 K [22–25]. Mg_2SnO_4 has a similar crystal structure to $MgAl_2O_4$ with the same space group No. 227 ($Fd\bar{3}m$). The tetravalent Sn ions are located only at octahedral sites; while one half of the divalent Mg ions occupy octahedral sites, and the other half occupy tetrahedral sites. The Sn ions and Mg ions at octahedral sties are arranged in a systematical disorder. Sn has a low neutron absorption cross section (0.626×10^{-28} m^2), which is desirable for IM materials. Moreover, the atomic weight of Sn is 118.710 g/mol and the ionic radius of Sn^{4+} (VI) is 0.69 Å [26], which makes Sn a much heavier and larger ion than Al^{3+} (VI). Since the main barrier to the motion of target atoms out of their original lattice positions and result in damage tracks is the existence of

* Corresponding author. Tel.: +1 (352) 846 3768; fax: +1 (352) 846 3355.
E-mail address: pengxu@ufl.edu (P. Xu).

0022-3115/$ - see front matter Published by Elsevier B.V.
doi:10.1016/j.jnucmat.2009.02.019

neighboring target atoms which are simply in the way, the compound with the same crystal structure but bigger and heavier atoms may be less susceptible to swift heavy ion damage. The inverse spinel structure also makes Mg_2SnO_4 interesting to study because very little is know about the irradiation stability of inverse spinel experimentally.

2. Experimental procedure

2.1. Specimen preparation

Mg_2SnO_4 samples were synthesized by calcining MgO (Cerac Inc. 99.95%) and SnO_2 (Alfa Aesar 99.9%) powder stoichiometrically at 1473 K for 12 h through conventional solid state processing. The obtained powder was loaded into a 13 mm punch and die-set and pressed into a cylindrical green pellet using Carver cold uniaxial press, and subsequently sintered in air at 1823 K for 24 h. The TEM specimens for *in situ* ion irradiation were prepared by crushing the ceramic samples or using focused ion beam (FIB). Using the former method, the calcined Mg_2SnO_4 powder was crushed in ethanol using a small agate mortar and pestle, and the suspension was subsequently dropped onto a carbon coated copper grid. Using the latter method, an electron transparent lamella was prepared with an FEI Strata DB 235 FIB/SEM dual-beam system. An auto-FIB script for TEM sample preparation was used and the sample was ion-milled until the desired thickness of ~200 nm was achieved. The specimen was then cut free and lifted out ex situ using an optical microscope and micromanipulators.

2.2. In situ ion irradiation and characterization

The irradiation tests and characterization were carried out at the IVEM-Tandem facility in the Electron Microscopy Center (EMC) at Argonne National Laboratory (ANL). Kr ions were used as the irradiation source, and were double-charged and accelerated to 1 MeV using a 650 kV NEC Ion Implanter. The irradiation tests were performed at cryogenic temperatures (50 and 150 K), using a liquid-helium-cooled cold stage. The temperature was monitored using a thermocouple attached to the sample holder near the sample position. *In situ* characterization was performed on a HITACHI H-9000NAR electron microscope operated at 300 kV. The electron beam traveled vertically down through the specimen and the irradiating ion beam was incident on the specimen at 30° to the vertical. TEM samples were irradiated at a dose rate between 10^{14} and 10^{16} Kr^{2+} ions/m^2/s. Periodically during the irradiation, the ion beam was shut off and the specimens were inspected *in situ* so that bright field (BF) images and selected-area electron diffraction (SAED) patterns could be recorded. The chemical compositions of TEM specimens were determined *ex situ* at room temperature using energy dispersive spectroscopy (EDS) on JOEL 2010F TEM in the Major Analytical Instrumentation Center (MAIC) at the University of Florida.

3. Results and discussion

3.1. TRIM based calculation

The average penetration depth of 1 MeV Kr^{2+} in Mg_2SnO_4 was calculated using the program TRIM-2008 (transport of ions in matter) [27]. The projected range of 1 MeV Kr^{2+} ions in Mg_2SnO_4 is about 370 nm, with a longitudinal straggling (defined as the square root of the variance, which is an average of the square of the deviations of the ion ranges from the mean projected range) of about 103 nm. Only the grains with grain size at or less than ~200 nm were chosen to be characterized for irradiation stability. The irradiation damage profile and ion implantation concentration as a function of target depth are plotted in Fig. 1. The TRIM calculation results indicate that at sample depths between 100 and 300 nm, the atomic displacement damage ranges from about 1.0 to 1.2 dpa per 10^{19} Kr^{2+} ions/m^2, averaged over the sublattices of spinel. A threshold energy for displacement is assumed to be 40 eV for Mg, Sn, and O based on values published in literature [28]. As indicated in Fig. 1, the concentration of implanted Kr ions at depth of 200 nm is about 0.0135 at% at ion fluence of 10^{19} Kr^{2+} ions/m^2. For the maximum fluence used in this experiment, the implanted Kr concentration is about 0.135 at% at depth of 200 nm.

3.2. Irradiation of Mg_2SnO_4 at 50 K

The FIB prepared Mg_2SnO_4 specimen was irradiated by 1 MeV Kr^{2+} ions to a maximum fluence of 5×10^{19} ions/m^2 at 50 K. A BF image of the entire specimen before irradiation is shown in Fig. 2(a). The specimen is a 15 × 6 μm electron transparent lamella with a thickness of ~ 200 nm. The dark strip on one side of this lamella is Pt, a foreign material that was coated to protect the surface of the sample from ion damage. The hole in the lamella originated from a pore inside the sintered Mg_2SnO_4 pellet. Two SAED patterns were recorded for areas *b* (0.1 dpa) and *c* (0 dpa) in the BF image and are shown in Fig. 2(b) and (c). The specimen was slightly tilted so that the electron beam direction was [1 1 4] for area *b* and [1 2 5] for area *c*. Fig. 2(d) shows a BF image of the specimen after irradiation by 1 MeV Kr^{2+} ions at an ion fluence of 5×10^{19} ions/m^2. It can be seen that the amorphous carbon film was extensively damaged by ion irradiation. Fig. 2(e) and (f) show the SAED patterns for areas *e* and *f* in the BF image after irradiation, which are the same locations as areas *b* and *c* in Fig. 2(a). As shown in Fig. 2(e) and (f), no diffraction spots can be seen, which indicates that the specimen was completely amorphisized. The BF image shows less contrast than the unirradiated sample, with the grain boundaries fading or disappearing. While the SAED patterns recorded at lower ion doses (10^{18} ions/m^2, 2×10^{18} ions/m^2, 5×10^{18} ions/m^2, 10^{19} ions/m^2 and 2×10^{19} ions/m^2) are not shown here, all of them show diffracted spots or diffused spots, suggesting that the specimen was not completely amorphisized at those ion fluences. Besides the two monitored areas, several grains of the specimen were examined at the ion influence of 5×10^{19} ions/m^2, and none of them showed diffraction spots. Therefore, the critical amorphization dose for Mg_2SnO_4 at the cryogenic temperature 50 K can be concluded as 5×10^{19} ions/m^2, which corresponds to an atomic displacement dose of approximately 5.5 dpa at a depth of ~200 nm.

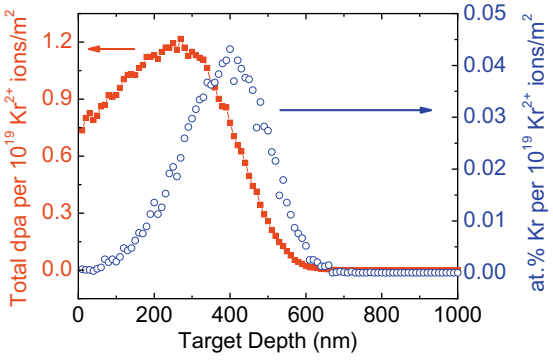

Fig. 1. TRIM simulations of total target atom displacements (averaged over all sublattices of the material) in dpa, and the concentration of implanted Kr ions, in Mg_2SnO_4 spinel as a function of target depth, for irradiations using 1 MeV Kr^{2+} ions. Values on the ordinates are normalized to a fluence of 1×10^{19} ions/m^2. TRIM simulations based on 10,000 ions.

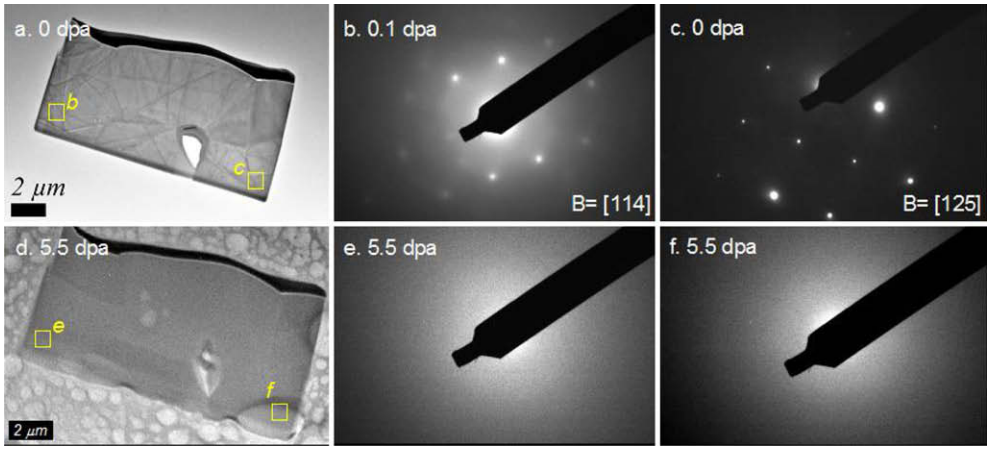

Fig. 2. FIB prepared Mg_2SnO_4 specimen: (a) BF image of the specimen before irradiation, (b) SAED pattern for area *b*, (c) SAED pattern for area *c*, (d) BF image of the specimen irradiated by 1 MeV Kr^{2+} to fluence of 5×10^{19} Kr^{2+} ions/m^2 (5.5 dpa), (e) SAED pattern for area *e*, and (f) SAED pattern for area *f*.

The liquid helium was released after irradiation and the specimen was warmed up to room temperature. The specimen was examined again using TEM on the next day in order to study the thermal annealing effects. Fig. 3(a) shows a BF image of the irradiated specimen at room temperature. The specimen was tilted in order to align the electron beam near zone axis for areas *b* and *c* in the BF image, which match the same locations as shown in Fig. 2. The SAED patterns were recorded and are shown in Fig. 3(b) and (c), which can be indexed as spinel Mg_2SnO_4 along [001] zone axis. The results indicate that the spinel crystal structure was formed at these regions, suggesting that annealing at room temperature is effective in thermally recovering the spinel crystalline phase from the fully amorphous Mg_2SnO_4. The emergence of grain boundaries in the BF image confirms that the annealed specimen is a polycrystalline material.

Nevertheless, a thin layer of ~600 nm in width was observed on the side of the sample (shown in Fig. 3(a)) after the irradiation and annealing. A BF image recorded for the area *d* (see Fig. 3(d)) shows a heterogeneous microstructure. Chemical analysis was performed using EDS and the collected spectra for areas *e* and *f* are shown in Fig. 3(e) and (f). The ion source of the FIB, Ga, was detected throughout the sample. Ga ion implantation and structural damage caused by FIB in the TEM sample preparation is a typically problem even though Ga ions travel at glancing angles of <1° on sample surface [29]. Semi-quantitative EDS analysis reveals that area *e* is a Sn depleted region with an atomic ratio of Mg to Sn about 20, and the dark precipitate at area *f* is a Sn rich region, with an atomic ratio of Mg to Sn about 1.7 (slightly lower than the expected 2:1 stoichiometry). Fig. 4 shows a SAED pattern recorded at the area *d*, where a polycrystalline ring pattern was obtained and can be indexed as MgO. Some diffraction spots cannot be identified as MgO, indicating that other crystalline phases are also present. The specimen was also annealed at 573 K for 0.5 h in a conventional oven but no significant change was observed. The formation of this segregation layer is not clear at this moment. Wang and his co-workers [14] have found spinel γ-$SiFe_2O_4$ first becomes amorphous and then crystallizes into Fe_3O_4 and SiO_2 under continued Kr^+ irradiation at 873 K, and they attributed it to the high pressure metastable phase of -$SiFe_2O_4$. However, this is unlikely the case for Mg_2SnO_4 because the thermal recovery of spinel structure was achieved elsewhere and confirmed by SAED patterns as shown in Fig. 3. This segregation layer could be the result of surface contamination by implanted Ga^+ ions during FIB preparation. It may also be formed during irradiation as a result of differential Mg and Sn sputtering followed by non-stoichiometric crystallization at room temperature. Further investigation is needed to elucidate the formation of this segregation layer.

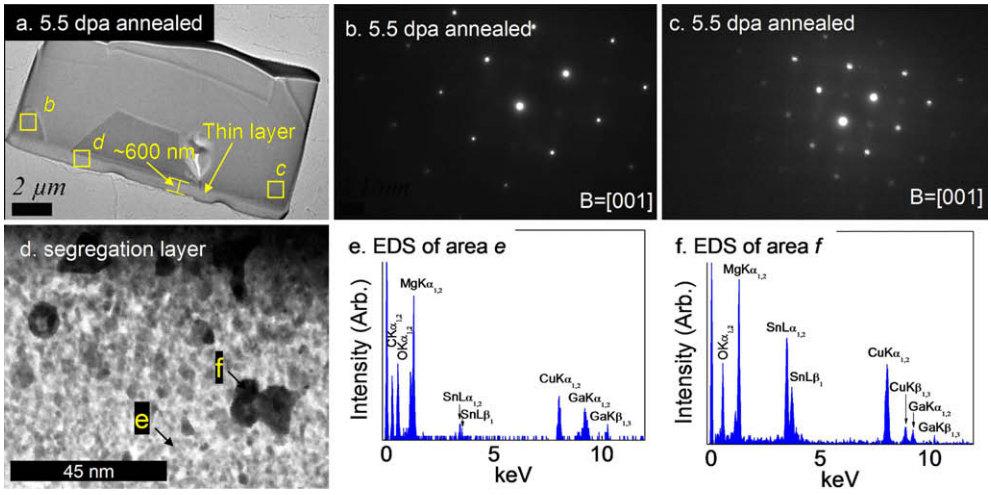

Fig. 3. The Mg_2SnO_4 sample irradiated by 1 MeV Kr^{2+} at a fluence of 5×10^{19} Kr^{2+} ions/m^2 at 50 K and structure was thermally recovered at room temperature: (a) BF image, (b) SAED pattern for area *b*, (c) SAED pattern for area *c*, (d) BF image of area *d*, (e) EDS spectra of area *e* and (f) EDS spectra for area *f*.

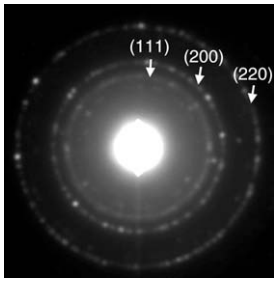

Fig. 4. SAED pattern recorded on the segregation layer. A ring pattern from polycrystalline materials is obtained and can be index as crystalline MgO. Several diffraction spots are not located on the rings, indicating other crystalline materials are also present.

3.3. Irradiation of Mg_2SnO_4 at 150 K

Crushed Mg_2SnO_4 grains were irradiated at 150 K and six randomly orientated grains or grain clusters were chosen and monitored. The random orientations were chosen to avoid the potential effects of ion channeling. The SAED patterns were recorded at ion fluences of 0, 10^{19}, 5×10^{19} and 10^{20} Kr ions/m^2 and a series of patterns for a grain cluster are shown in Fig. 5. The orientation of grains usually changes after ion irradiation, which is probably due to buckling of the carbon film as a result of ion-induced breakdown of formvar which comes from the film fabrication [30]. The presence of diffracted spots in the SAED patterns in Fig. 5(b) and (c) indicates that the specimen was not completely amorphized at those ion fluences. The diffraction spots vanished finally at an ion fluence of 10^{20} ions/m^2, which is equivalent to an atomic displacement damage of about 11.0 dpa for grains with a diameter of ~200 nm. The specimen was translated and several other grains were examined using SAED after the final ion dose. It was observed that approximately one out of five grains was not amorphous and still retained crystallinity. A similar case was also reported by Smith and his co-workers [30]; and the grains that cannot be amorphisized are referred to as outliers. Several possible explanations are given in Smith's paper [30] for the existence of outliers, but the most likely scenario in this case is that the elevated temperatures due to poor thermal connection between the outliers and the carbon film cause annealing of irradiation damage [31]. Therefore, the outliers were not considered in determining the amorphization dose, which was then concluded to be 11.0 dpa for Mg_2SnO_4 at 150 K.

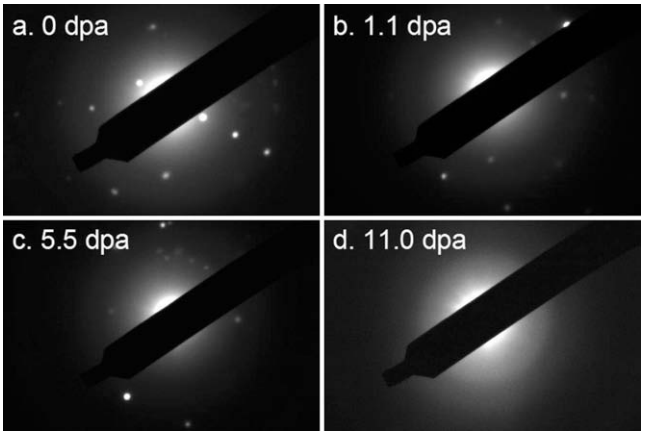

Fig. 5. SAED patterns of the crushed Mg_2SnO_4 grains irradiated at 150 K: (a) prior to ion irradiation and (b)–(d) following exposure to 1.0 MeV Kr^{2+} ions to fluences of 10^{19} (1.1 dpa), 5×10^{19} (5.5 dpa), and 10^{20} (11.0 dpa) Kr^{2+} ions/m^2, respectively.

Since defects created by ion irradiation can be annihilated by the thermal annealing process, the irradiation stability of a material is expected to be improved at elevated temperatures [32]. As a result, the amorphization dose should increase with irradiation temperatures because the thermal annealing becomes more efficient in restoring crystallinity. The temperature dependence of amorphization is a result of the competition between amorphization and recovery processes. It is worth noting that the geometries of the samples irradiated at 50 and 150 K are different: the one irradiated at 50 K is a thin slab cut out from a sintered polycrystalline Mg_2SnO_4 using FIB and the one irradiated at 150 K are a bundle of crushed particles. Nevertheless, the amorphization dose for Mg_2SnO_4 increases from 5.5 to 11.0 dpa as the irradiation temperature increases from 50 to 150 K, regardless the geometry of the specimens.

3.4. Irradiation damage mechanism of Mg_2SnO_4 by 1 MeV Kr^{2+}

It is known that the energy loss of energetic ions in target atoms is mainly due to electronic scattering and nuclear scattering [33]. The partitioning of energy transferred into electronic scattering and nuclear scattering is an important process controlling the effect of irradiation [34]. In order to study the irradiation damage mechanisms of 1 MeV Kr^{2+} ions in the inverse spinel Mg_2SnO_4, the electronic and nuclear stopping powers were calculated using TRIM computer simulations and the results are presented in Fig. 6. It is shown that the electron stopping power, $(dE/dX)_e$ (the peak value ~1.5 keV/nm/ion at the sample depth of 200 nm), exceeds the nuclear stopping, $(dE/dX)_n$ (the peak value ~1.0 keV/nm/ion at the sample depth of 300 nm), except at the end of range of ions. The results indicate that both nuclear (ballistic) scattering events and electronic (ionization) scattering events play important roles on the ion-solid interaction. Since fission tracks have not been observed and the deposition rate for the electronic scattering is only above 1 keV/nm, the Coulomb explosion and thermal spike are not likely to be the dominant damage mechanisms even though the electronic stopping power exceeds the nuclear stopping power [35,36]. As a result, the major damage mechanism is the atomic displacement induced defect accumulation.

3.5. Irradiation tolerance of Mg_2SnO_4

Since most studies have focused on the irradiation behavior of $MgAl_2O_4$, the critical amorphization doses for other spinel compounds are not well known. It has been reported that the amorphization dose is ~4 dpa for $FeCr_2O_4$ at 20 K and 0.2 dpa for γ-SiFe2O4 below 723 K [14]. Mg_2SnO_4 exhibits a moderate irradi-

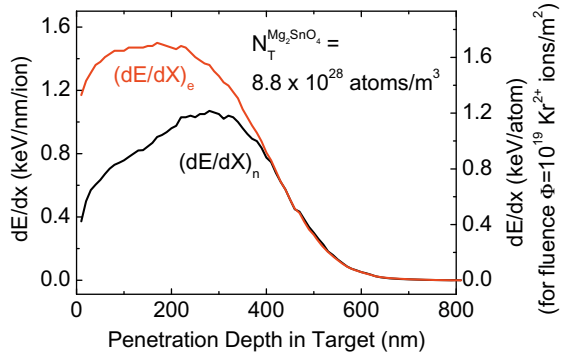

Fig. 6. Electronic $((dE/dx)_e)$ and nuclear $((dE/dx)_n)$ stopping powers for 1 MeV Kr^{2+} ions in the Mg_2SnO_4 target based on TRIM simulation results. The figure is plotted in two types of units: [keV/nm/ion] and [eV/atom], the latter for an arbitrary fluence of $\Phi = 10^{19}$ Kr^{2+} ions/m^2.

ation resistance against ion damage at intermediate energies (typically a few MeV), but the ability to annihilate atomic displacement induced defects is not as good as the normal spinel $MgAl_2O_4$ [8,14,37].

There are several factors which could explain the different irradiation resistances of Mg_2SnO_4 and $MgAl_2O_4$. The first consideration is the atomic arrangement in the structure and cation inversion. Based solely on structural considerations, recovery of damage will be better in an isotropic crystal compared with an anisotropic one [17]. Similar to other inverse spinel compounds, Mg_2SnO_4 has a random distribution of Mg^{2+} and Sn^{4+} cations on the octahedral sites, which contributes to changes in bond lengths locally in the structure and results in some degree of anisotropy. Computer simulations have been done to study the irradiation responses of different spinel compounds with varying inversion including the normal $MgAl_2O_4$, the half-inverse $MgGa_2O_4$ and the fully inverse $MgIn_2O_4$ [17,18]. Bacorisen and co-workers [17] have used molecular dynamics (MD) to simulate collision cascades and found out that the irradiation induced damage to the structure is more extensive for the fully inverse $MgIn_2O_4$ compared with the other two. Uberuaga and co-workers [18] have used temperature accelerated dynamics (TAD) to simulate and characterize the kinetics of defects for the same three spinel oxides in order to study the cation ordering effects. It is concluded that the cation disorder greatly complicates and inhibits the motion of point defects through the spinel structure, which leads to defect accumulation and less irradiation tolerance. Nevertheless, it might be misleading to correlate the irradiation behaviors purely with inversion because many other factors may also have large effects on irradiation tolerance.

The second consideration is the chemical bond effects. Trachenko and co-workers [38] have found that the irradiation stability is governed by the ionicity of bonding, with higher ionicity leading to more stable materials under irradiation. The ionicity of a chemical bond can be estimated using Pauling's electronegativity and indicated by the difference of electronegativity between a cation and an anion [39]. The relative electronegativities determined by Pauling for Mg, Sn (IV), Al and O are 1.31, 1.96, 1.61 and 3.44, respectively. The electronegativities were further modified by Batanov [40] for crystalline compounds with a consideration of the valence state and the coordination of atoms, and the obtained values for Mg, Sn (IV), Al and O are 0.8, 2.0, 1.4 and 3.2, respectively. The difference of electronegativity between Sn and O is smaller than Al and O and also smaller than Mg and O, suggesting that the covalency of ⟨Sn–O⟩ bond is higher than ⟨Al–O⟩ and ⟨Mg–O⟩, and Mg_2SnO_4 is more covalently bonded than $MgAl_2O_4$. Similarly in pyrochlore stannate compounds, high covalency of ⟨Sn–O⟩ bond has also been found both experimentally using neutron and X-ray diffraction and theoretically using density functional theory (DFT) computer simulation [41–44]. Therefore, the high covalency of ⟨Sn–O⟩ bond in Mg_2SnO_4 may cause the structure more susceptible to irradiation damage than $MgAl_2O_4$.

The third consideration is cation defect formation ability. It has also been shown that irradiation tolerance of complex oxide compounds is dependent on the ability to accommodate cation disorders [9]. Sickafus and co-workers [45] have observed a significant amount of cation disorders in the normal spinel $MgAl_2O_4$ upon neutron exposure in excess of 50 dpa at 670 K. The ability to accommodate cation disorders can be inferred from the cation antisite defect energy, which mainly depends on the difference in cation radii. In normal spinel $MgAl_2O_4$, the ionic radii of Mg^{2+} at tetrahedral sites and Al^{3+} at octahedral sites are 0.57 and 0.535 Å, respectively. In the inverse spinel Mg_2SnO_4, the ionic radii of Mg^{2+} at tetrahedral sites and Sn^{4+} at octahedral sites are 0.57 and 0.69 Å, respectively. All ionic radii are obtained from Shannon [26]. The ionic radius ratio of r_B/r_A for $MgAl_2O_4$ and Mg_2SnO_4 are calculated to be 0.94 and 1.21, which indicates that the cation radii difference in Mg_2SnO_4 is larger than in $MgAl_2O_4$. Moreover, Sn^{4+} is a tetravalent ion and Al^{3+} is a trivalent ion. Swapping between Sn^{4+} and Mg^{2+} will most likely cause more lattice instability or distortion due to the greater charge difference. The spinel structure is also well known for its abundant structural vacant sites on both tetrahedral positions (87.5% are vacant) and octahedral positions (50% are vacant). The large fraction of vacancy sites in the structure is responsible for effective interstitial–vacancy (i–v) recombination, which is also an important mechanism for annihilation of point defects created by irradiation. Nevertheless, $MgAl_2O_4$ and Mg_2SnO_4 both have equal numbers of vacancy sites in their structures, and it is not likely to become an important factor that results in different irradiation tolerances.

Overall, Mg_2SnO_4 is not as resistant as $MgAl_2O_4$ against ballistic displacements under intermediate energy ion irradiation. Since the stopping power for swift heavy ions traversing in solids is mainly electronic stopping, which is a different damage mechanism, it is useful to conduct high energy ion irradiation to further evaluate the irradiation stability of Mg_2SnO_4 and compare it with $MgAl_2O_4$.

4. Conclusions

Magnesium stannate was irradiated with 1.0 MeV Kr^{2+} ions at 50 and 150 K to a maximum fluence of 5×10^{19} Kr ions/m^2 and 10^{20} Kr ions/m^2, respectively. Microstructure and crystal structure evolutions were monitored and recorded *in-situ* by BF images and SAED patterns. The amorphization doses for Mg_2SnO_4 irradiated by 1.0 MeV Kr^{2+} ions at 50 and 150 K were determined to be 5×10^{19} Kr ions/m^2 and 10^{20} Kr ions/m^2, which correspond to an atomic displacement of 5.5 and 11.0 dpa, respectively. The spinel crystalline structure was thermally recovered at room temperature from the amorphous Mg_2SnO_4 which was irradiated at 50 K. The electronic stopping power exceeds the nuclear stopping power except the end of range of ions, but is only ~1.5 keV/nm. This suggests that the amorphization phenomenon observed in this study is mainly due to atomic displacement induced defect accumulation. Mg_2SnO_4 shows less irradiation resistance compared with $MgAl_2O_4$ against ballistic displacement damage, which can be attributed to its inverse structure, higher covalency of the ⟨Sn–O⟩ bond, larger ionic size and charge difference between Mg^{2+} and Sn^{4+}.

Acknowledgements

The authors wish to thank E.A. Ryan, P. Baldo, A. Liu and M. A. Kirk, IVEM-Tandem Facility staff at ANL, for their assistance with ion irradiations. The authors would also like to thank the technical assistance from the Major Analytical Instrumentation Center (MAIC), Department of Materials Science and Engineering, University of Florida. This work is funded by the US Department of Energy through the Nuclear Energy Research Initiative (NERI) Program (DE-FC07-05ID14647).

References

[1] C. Degueldre, J.M. Paratte, J. Nucl. Mater. 274 (1999) 1.
[2] M. Burghartz, H. Matzke, C. Leger, G. Vambenepe, M. Rome, J. Alloy Compd. 271 (1998) 544.
[3] K. Nakai, K. Fukumoto, C. Kinoshita, J. Nucl. Mater. 191 (1992) 630.
[4] F.W. Clinard, G.F. Hurley, L.W. Hobbs, J. Nucl. Mater. 108 (1982) 655.
[5] L.W. Hobbs, F.W. Clinard, S.J. Zinkle, R.C. Ewing, J. Nucl. Mater. 216 (1994) 291.
[6] C. Kinoshita, K. Fukumoto, K. Fukuda, F.A. Garner, G.W. Hollenberg, J. Nucl. Mater. 219 (1995) 143.
[7] S.J. Zinkle, J. Am. Ceram. Soc. 72 (1989) 1343.
[8] K.E. Sickafus, N. Yu, M. Nastasi, J. Nucl. Mater. 304 (2002) 237.
[9] K.E. Sickafus, L. Minervini, R.W. Grimes, J.A. Valdez, M. Ishimaru, F. Li, K.J. McClellan, T. Hartmann, Science 289 (2000) 748.
[10] K.E. Sickafus, N. Yu, R. Devanathan, M. Nastasi, Nucl. Instrum. Meth. B 106 (1995) 573.

[11] T. Wiss, H. Matzke, Radiat. Meas. 31 (1999) 507.
[12] T.A.G. Wiss, P.M.G. Damen, J.P. Hiernaut, C. Ronchi, J. Nucl. Mater. 334 (2004) 47.
[13] F.C. Klaassen, K. Bakker, R.P.C. Schram, R.K. Meulekamp, R. Conrad, J. Somers, R.J.M. Konings, J. Nucl. Mater. 319 (2003) 108.
[14] L.M. Wang, W.L. Gong, S.X. Wang, R.C. Ewing, J. Am. Ceram. Soc. 82 (1999) 3321.
[15] D. Simeone, C. Dodane-Thiriet, D. Gosset, P. Daniel, M. Beauvy, J. Nucl. Mater. 300 (2002) 151.
[16] G. Baldinozzi, D. Simeone, D. Gosset, S. Surble, L. Mazerolles, L. Thome, Nucl. Instrum. Meth. B 266 (2008) 2848.
[17] D. Bacorisen, R. Smith, B.P. Uberuaga, K.E. Sickafus, J.A. Ball, R.W. Grimes, Phys. Rev. B 74 (2006) 214105.
[18] B.P. Uberuaga, D. Bacorisen, R. Smith, J.A. Ball, R.W. Grimes, A.F. Voter, K.E. Sickafus, Phys. Rev. B 75 (2007) 104116.
[19] F. Studer, M. Hervieu, J.M. Costantini, M. Toulemonde, Nucl. Instrum. Meth. B 122 (1997) 449.
[20] M. Treilleux, G. Fuchs, A. Perez, E. Balanzat, J. Dural, Nucl. Instrum. Meth. B 32 (1988) 397.
[21] C. Houpert, M. Hervieu, D. Groult, F. Studer, M. Toulemonde, Nucl. Instrum. Meth. B 32 (1988) 393.
[22] G. Pfaff, Thermochim. Acta 237 (1994) 83.
[23] W.W. Coffeen, J. Am. Ceram. Soc. 36 (1953) 207.
[24] A.M. Azad, L.J. Min, Ceram. Int. 27 (2001) 325.
[25] I.N.S. Jackson, Rc. Lieberma, A.E. Ringwood, Earth Planet Sci. Lett. 24 (1974) 203.
[26] R.D. Shannon, Acta Crystallogr. A 32 (1976) 751.
[27] J.F. Ziegler, J.P. Biersack, U. Littmark, The Stopping and Range of Ions in Solids, New York, 2008.
[28] G.P. Pells, J. Nucl. Mater. 155 (1988) 67.
[29] J. Mayer, L.A. Giannuzzi, T. Kamino, J. Michael, MRS Bull. 32 (2007) 400.
[30] K.L. Smith, N.J. Zaluzec, G.R. Lumpkin, J. Nucl. Mater. 250 (1997) 36.
[31] W.J. Weber, R.C. Ewing, L.M. Wang, J. Mater. Res. 9 (1994) 688.
[32] W.J. Weber, Nucl. Instrum. Meth. B 166 (2000) 98.
[33] R. Devanathan, N. Yu, K.E. Sickafus, M. Nastasi, Nucl. Instrum. Meth. B 127 (1997) 608.
[34] W.J. Weber, R.C. Ewing, C.R.A. Catlow, T.D. de la Rubia, L.W. Hobbs, C. Kinoshita, H. Matzke, A.T. Motta, M. Nastasi, E.K.H. Salje, E.R. Vance, S.J. Zinkle, J. Mater. Res. 13 (1998) 1434.
[35] Rl. Fleische, P.B. Price, R.M. Walker, J. Appl. Phys. 36 (1965) 3645.
[36] S.J. Zinkle, V.A. Skuratov, Nucl. Instrum. Meth. B 141 (1998) 737.
[37] N. Bordes, L.M. Wang, R.C. Ewing, K.E. Sickafus, J. Mater. Res. 10 (1995) 981.
[38] K. Trachenko, J.M. Pruneda, E. Artacho, M.T. Dove, Phys. Rev. B 71 (2005) 184104.
[39] L. Pauling, The Nature of the Chemical Bond, Ithaca, NY, 1960.
[40] S.S. Batsanov, Zh. Neorg. Khim+ 20 (1975) 2595.
[41] Z.J. Chen, H.Y. Xiao, X.T. Zu, L.M. Wang, F. Gao, J. Lian, R.C. Ewing, Comput. Mater. Sci. 42 (2008) 653.
[42] J. Lian, R.C. Ewing, L.M. Wang, K.B. Helean, J. Mater. Res. 19 (2004) 1575.
[43] B.J. Kennedy, B.A. Hunter, C.J. Howard, J. Solid State Chem. 130 (1997) 58.
[44] J. Lian, K.B. Helean, B.J. Kennedy, L.M. Wang, A. Navrotsky, R.C. Ewing, J. Phys. Chem. B 110 (2006) 2343.
[45] K.E. Sickafus, A.C. Larson, N. Yu, M. Nastasi, G.W. Hollenberg, F.A. Garner, R.C. Bradt, J. Nucl. Mater. 219 (1995) 128.